Available online at www.CivileJournal.org

Civil Engineering Journal

(E-ISSN: 2476-3055; ISSN: 2676-6957)

Vol. 12, No. 05, May, 2026

Evaluation of Double-Vacuum Saturation in Triaxial Testing of Compacted Clay: A Comparison with Back-Pressure Methods

Muhammad Riza [1], H. Nawir [1*], E. Rismantojo [1], Fourier D. E. Latief [2]

[1] *Faculty of Civil and Environmental Engineering, Institut Teknologi Bandung, Bandung 40132, Indonesia.*

[2] *Faculty of Mathematics and Natural Sciences, Institut Teknologi Bandung, Bandung 40132, Indonesia.*

Received 08 August 2025; Revised 22 March 2026; Accepted 08 April 2026; Published 01 May 2026

Abstract

Achieving full saturation in consolidated triaxial testing is challenging, especially for compacted and residual soils with low water content and complex microstructures. Conventional back-pressure saturation can cause disturbance and leaching, leading to unreliable results. This study evaluates the double-vacuum (DV) method to reduce sample disturbance and better preserve microstructure during testing of compacted kaolin clay. Two methods—back pressure (NV) and double-vacuum (DV)—were compared using the consolidated undrained triaxial test and micro-CT imaging. The DV method reached a Skempton B-value ≥ 0.95 at lower pressure (150-200 kPa) in 8 hours, while NV needed up to 450 kPa and 50 hours. The DV approach halved axial and radial deformation and resulted in lower changes in void ratio ($\Delta e/e_0 \approx 0.055$), indicating improved sample integrity. Micro-CT showed a more uniform pore distribution and lower residual porosity (0.43%) versus NV (1.04%). These results suggest the DV method is a more reliable, less intrusive way to prepare fine-grained soils for triaxial testing, with significant implications for geotechnical labs, especially where high-pressure systems are limited.

Keywords: Dry Saturation Method; Back Pressure, Disturbance; Micro-CT; Microstructures.

1. Introduction

Achieving full saturation in Triaxial Consolidated Undrained testing is challenging. Certain soils, such as compacted or remolded samples, those at optimum moisture content (OMC), and residual soils, often have low natural water content. This challenge arises because residual soils are generally unsaturated and typically sit above the water table. Consequently, achieving a high degree of saturation requires increased time and higher pressure [1–5]. In soils whose mechanical behavior depends on structure and mineralogy (such as residual soils and stiff clay) saturation and reconsolidation can modify the microstructure. This leads to sample disturbance and affects the mechanical behavior observed in consolidated undrained triaxial tests [6–8]. The degree of sample disturbance and quality control is generally measured by the pore number ratio ($\Delta e/e_0$) during reconsolidation, as identified by Lunne et al. [9]. However, void ratio (e_0) only represents the relationship between void volume (V_v) and solid volume (V_s), and does not directly reflect the total actual void volume. Technological advances, such as micro-computed tomography (micro-CT), now enable more accurate visualization of pore distribution and particle interactions. This technique provides enhanced microstructural insights into the mechanisms of saturation and reconsolidation, and their impact on the mechanical characteristics observed in consolidated undrained triaxial tests.

* Corresponding author: hasbi@itb.ac.id

https://doi.org/10.28991/CEJ-2026-012-05-04

In conventional triaxial testing, the saturation method applies back pressure to compress air voids and dissolve air pores into water, while maintaining a higher cell pressure to prevent specimen bulging. However, repeated use of back-pressure during consolidated undrained triaxial testing may damage structural integrity [10] and cause leaching processes [11]. Mineral leaching lowers the shear strength of the natural clay [8, 12–14]. If saturation damages the soil structure, reconsolidation cannot restore the in-situ effective stress; this method is only effective if there is no structural damage [15]. Besides, the small-strain stiffness (G_0) in clays and sands is also known to depend on mean effective stress through a power-law relationship, with parameters that reflect soil structure [8]. Therefore, analyzing the mechanical behavior and key parameters of structured soils, such as residual soils and stiff clays, helps clarify how their structures evolve. The double-vacuuming saturation method was first described by Donaghe & Townsend [1] and later introduced by Rad & Wayne Clough [16]. It is common in Japan and is included in the Japanese Geotechnical Society Standard [17], as cited in ASTM D4767-11 [18]. This process, also called the dry-saturation method, is used to saturate sandy soils under low back pressure. The method achieves high saturation using lower back pressure (100-200 kPa), while conventional methods require 400–800 kPa for soils with low initial saturation. High back pressure limits the practical application of stress during consolidation and shear loading, and industrial pneumatic systems and triaxial cells are usually limited to 7–8 bars (700-800 kPa).

Numerous studies have employed the double-vacuum saturation method to analyze the mechanical behavior of sand [16, 19–22], clay [5, 17, 19, 23], and residual soil [11, 22, 24–29]. All researchers have shown that the vacuum saturation method is more effective than the conventional back-pressure technique. It achieves faster saturation, produces a lower final back pressure, and reaches a degree of saturation at least a B-skempton value of 0.95. However, only a few studies [5, 17, 23] have examined the impact of the double-vacuum saturation method on sample disturbance, which in turn affects soil mechanical behavior. Yilmaz et al. [5] performed unconsolidated undrained triaxial tests on a 35 mm-diameter compacted clay sample, saturated by single vacuum (-70 kPa) and gravity (falling head) for 1 to 4 weeks. The saturation system was independent of the testing apparatus, so the Skempton B-value could not be controlled. Their results showed that one week of vacuum saturation produced lower strength than four weeks of gravity saturation, likely because free air prevented complete saturation and increased cohesion. Teng & Ou [23] used a suction control system with venturi vacuum generators in triaxial tests on 50 mm-diameter samples. They performed K_0-consolidated undrained axial compression (CK_0UAC) tests and a bender element test on reconstituted Taipei silty clay, with and without suction control. Results showed that suction control produced higher-quality specimens with lower $\Delta e/e_o$ values. Specimens saturated with suction control were classified as good to fair, while those without were fair to poor. Young's modulus and shear modulus were underestimated by 20% and 14%, respectively, in conventional saturation, indicating that stress-strain behavior at small strains is influenced by soil structure changes induced by the saturation method. This study focused on stiffness and undrained shear strength parameters, rather than stress-strain curve features or stress path behavior under different saturation methods.

Ampadu & Tatsuoka [17] studied reconstituted kaolin and in-situ stiff clay using dry saturation with a double-vacuum, and the conventional wet-setting method in consolidated undrained triaxial tests. At low stress, a wet setting produces softer specimens, which can lead to inaccurate pre-consolidation stress measurements. The setting procedure generally does not affect undrained strength beyond pre-consolidation pressure, unless effects are severe. Higher stress consolidation can erase setting impacts. However, this study does not address microstructural changes and their effects on shear strength using saturation methods. It should be noted that all studies measured disturbance using the pore ratio $\Delta e/e_0$, as described by Lunne et al. [9, 30], but they did not explore how the double-vacuum method influences disturbance at the microstructural level. This issue is critical in soils with complex structure and mineralogy, such as residual soils and stiff clays. Their disturbance criteria [9,30] were developed for marine clay or sedimentary soils, while research based on microstructural analysis using double-vacuum saturation in triaxial testing of volcanic residual soils remains very limited.

Recent research on microstructure changes caused by saturation or infiltration generally uses scanning electron microscopy (SEM) [31], mercury intrusion porosimetry (MIP) [32] and micro-computed tomography (micro-CT) [33, 34]. Zhuang et al. [34] investigated microstructural changes in loess soil after water-saturation infiltration using micro-CT, finding that porosity increased by about 20%. The pore-area ratio of the mesopores and macropores increased more than that of the micropores. Additionally, the number of small pores grew to more than 5 times that in the undisturbed loess. An et al. [33] simulated seepage in granite residual soil by dry-wet cycling based on micro-CT. The results showed mesopore structural changes that increased permeability. Small pores in the original sample expanded and connected after drying and wetting. Cracks and macropore volumes increased, while micropore volume decreased. Under dry-wet cycles, many small pores gradually transformed into large, highly connected cracks. This seepage simulation using micro-CT results can estimate the permeability characteristics of granite residual soil.

Optical microscopes and SEM capture only two-dimensional images. Outcomes depend on the observation direction [34–37]. The MIP technique may damage samples, and pore-size data may not reflect the actual size distribution [32,34]. In contrast, Micro-CT imaging can accurately display geometric features of particles and pores. It offers three-dimensional reconstruction and visualization. This technique provides non-destructive, quantitative, reproducible, and high-resolution analysis [32, 34, 38, 39]. However, only a few studies have used micro-CT to analyze microstructural changes from the double-vacuum saturation process during triaxial testing of volcanic residual soils.

In Indonesia, this method is used infrequently. The primary challenges impeding its development include limitations in equipment availability, capacity, and familiarity with the technique. Consequently, this study aims to adapt the double-vacuum method to these existing constraints while ensuring its applicability to achieve optimal results and promote further development in Indonesia. To address this gap, it is necessary to investigate the impact of the double-vacuum saturation method on the mechanical behavior of volcanic residual soil during consolidated undrained triaxial testing, using microstructure analysis derived from micro-CT results. The key research questions were as follows: (i). What is the effect of the double vacuum saturation method on the disturbance level of soil samples in general, and specifically from a microstructural perspective? (ii). How does the double vacuum saturation method influence the outcomes of consolidated undrained triaxial tests, particularly for soils whose mechanical behavior is affected by structure and mineralogy? This study is a preliminary study to answer the first research question. Therefore, to reduce the influence of the sample variation factors, consolidated undrained triaxial tests were performed on compacted kaolin clay soil samples with and without vacuum control. The research questions related to volcanic residual soil will be discussed in future studies. The porosity distribution, time required, level of disturbance, magnitude of the final pressure during saturation, consolidation characteristics, and stress-strain characteristics of kaolin clay were compared to examine the influence of the double-vacuum saturation process on changes in soil characteristics. The difference in the hydraulic gradient height during saturation is also discussed to determine the effect of the vacuum system on changes in soil characteristics.

This paper is divided into four sections. Section 1 covers background, the theoretical framework, literature review, gap analysis, novelty, and the research objective. Section 2 describes the materials, sample preparation, and experimental procedures, including the double-vacuum (DV) and back-pressure (NV) saturation systems, triaxial CU testing, and micro-CT analysis. Section 3 discusses results, focusing on the DV method's effect on saturation efficiency, deformation, disturbance, microstructure, hydraulic gradient, and the influence of saturation method on stress-strain behavior. Section 4 summarizes key findings and suggests future research directions for residual or reconstituted soils with high compressibility and sensitive material.

This study is expected to provide an overview of the double-vacuum method, specifically from a microstructural perspective, as an alternative to accelerate saturation, reduce the final pressure, and minimize sample disturbance during subsequent saturation studies.

2. Material & Testing Methods

Figure 1 shows the workflow diagram of the research methodology used in this study. In general, there are five stages to achieve the goal of this research, as detailed below:

- Material preparation
- Double-vacuum and back-pressure saturation Process
- Triaxial consolidation undrained test
- Micro-computed tomography (Micro-CT)
- Data Analysis

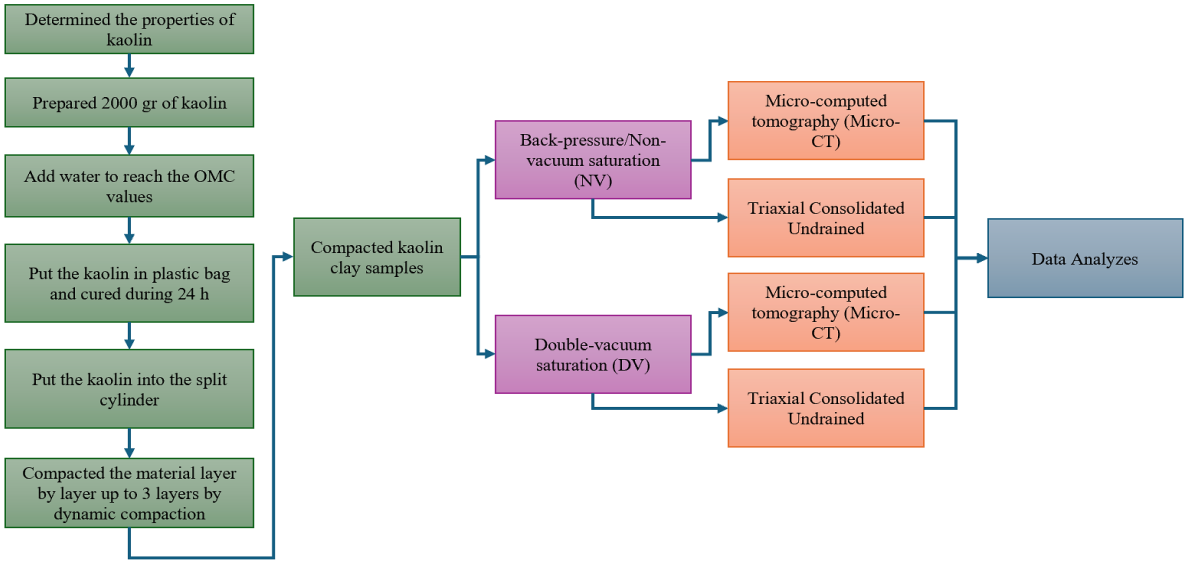

Figure 1. Research methodology

2.1. Kaolin Clay

To maintain a high level of homogeneity and mitigate uncertainties associated with the test material, this study utilized processed kaolin clay produced explicitly by PT. Yudian Kawan Mineral, Belitung, Indonesia, as shown in Figure 2. Table 1 shows the index properties, Atterberg limits, and grain size distribution of the kaolin clay material, providing the following results:

Figure 2. Kaolin clay, a product of PT. Yudian kawan mineral, Belitung, Indonesia

Table 1. Properties of kaolin clay

Item	Unit	Value
Material		Kaolin
Distributor		PT. Yudian Kawan Mineral
Specific gravity, Gs	-	2.58
Liquid Limit, LL	%	68.48
Plastic Limit, PL	%	37.88
Plasticity Index, PI	%	30.6
Clay	%	57.61
Silt	%	42.39
Sand	%	0
Gravel	%	0
D_{10}	mm	-
D_{30}	mm	0.0015
D_{60}	mm	0.003
C_u	-	-
C_c	-	-
Soil Classification, USCS	-	MH

2.2. Sample Preparation

Kaolin clay weighing 2,000 g was mixed with 600 mL of de-aired water (30%). The mixture was then cured for 24 h to ensure an even distribution of water content throughout the kaolin clay and to attain equilibrium moisture conditions. Using the standard Proctor method, the kaolin material was compacted and shaped in a stainless steel split compaction mold. The mold, measuring 70 mm in diameter and 140 mm in height, was designed for placement within the triaxial cell. A split compaction mold was used to minimize sample disturbance and reduce water content during trimming when forming the triaxial specimen. To prevent compression during sample extraction, a split-compaction mold was designed as a split tube, as illustrated in Figure 3.

Figure 3. Sample preparation process

2.3. Compaction Method

The prepared kaolin clay material was weighed and placed in a split mold in three layers, with each layer compacted by 29 blows using a hammer weighing 1.83 kg, with a diameter of 70 mm and a drop height of 200 mm, equivalent to the standard Proctor energy of ±597 kN-m/m^3 as shown in Figure 4 . Before applying each new layer, a kerf was created in the previous layer to ensure continuity of interlayer connections. As previously mentioned, a split-compaction mold was used to minimize sample disturbance and water content reduction during triaxial specimen formation. Furthermore, to prevent compression during sample extraction, a split compaction mold was designed as a split tube. This method follows ASTM D4767-11 [18] for preparing samples for triaxial testing, and has been utilized by several researchers for both dynamic and static compaction [40–44] on residual soil and other sensitive soils.

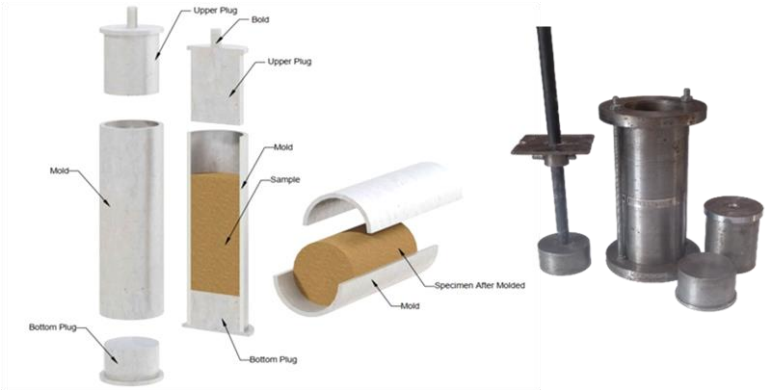

Figure 4. Schematic diagram of split tube compaction mold 70 mm diam. and 140 mm height

2.4. Double Vacuum Saturation Method System

In this study, two saturation methods were examined: (1) the back-pressure (NV) method and (2) the double-vacuum (DV) method. The commonly used back-pressure method was not further elaborated upon in this study. The double-vacuum method was implemented using a suction generator (convum), as illustrated in Figure 5, because standard vacuum machines were unable to maintain a continuous vacuum. The double-vacuum method used in this study is based on the work of Ampadu & Tatsuoka [17]. However, the maximum applied vacuum pressure was -80 kPa. This adjustment was made to accommodate the maximum capacity of compressor machines commonly used in Indonesia. The schematic diagram of a double-vacuum saturation system is shown in Figure 6. The saturation process using the double-vacuum method was conducted according to the following procedure and summarized in Table 2:

- **Stage I**: The vacuum pressure within the specimen was increased to -20 kPa, maintaining a constant vacuum pressure differential of 20 kPa between the outside and inside of the specimen. Open valve A until air bubbles stop rising in water tank A.
- Valve B was gradually opened to maintain the equilibrium of the vacuum pressure distribution across the specimen. At this stage, air bubbles appear in water tank A.
- Once the air bubbles disappeared, the vacuum pressure was increased to the subsequent stage **(Stage II to Stage IV)** while maintaining a constant vacuum pressure differential of 20 kPa. This process was repeated incrementally until the maximum achievable vacuum pressure was achieved. Compressors with a maximum capacity of 8 bar, commonly employed in soil mechanics laboratories in Indonesia, generate a suction pressure of -80 kPa. A higher maximum suction value can be achieved in this final process, thereby accelerating saturation and achieving a B-value ≥ 0.95.
- At maximum vacuum pressure **(Stage IV),** the vacuum process was continued until stable conditions were achieved (no air bubbles were detected).
- Upon achieving stable conditions, with the vacuum pressure maintaining its maximum level at a constant differential (20 kPa), the valve was closed in water tank B, elevating it 70 cm above water tank A. In this configuration, the valve at the bottom of water tank B was opened, allowing water from water tank B to flush towards the sample. This process was continued until water began to flow from the upper sample. During this process, the water flowing within the specimen filled the voids and displaced the remaining air bubbles in the soil because the maximum vacuum pressure (-80 kPa) did not approach the atmospheric pressure (1 atm). This entire phase requires approximately 4.5 hours, or until water flows from the upper specimen flow path.
- In the subsequent phase **(Stage V to Stage VI),** the vacuum pressure was gradually reduced while maintaining a constant differential pressure of -20 kPa between the outside and inside of the specimen, until it returned to its initial condition.

- The final condition (**Stage VII**) was reached when the pressure outside the sample was 0 kPa and the pressure inside the sample remained at -20 kPa. At this point, the double-vacuum process was considered complete (the vacuum system was deactivated), and the procedure progressed to saturation using the back-pressure method

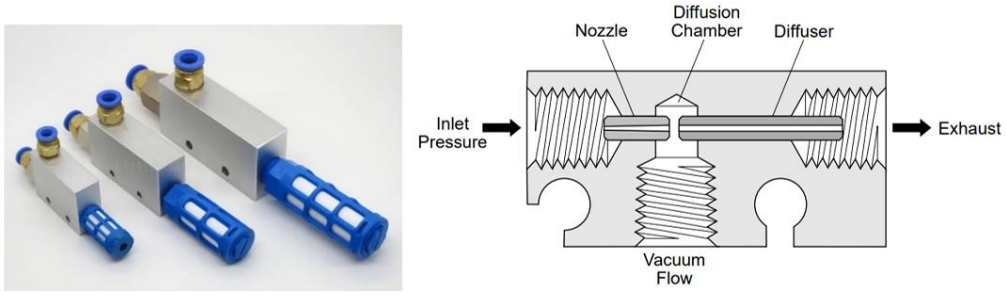

Figure 5. Suction generator/convuum

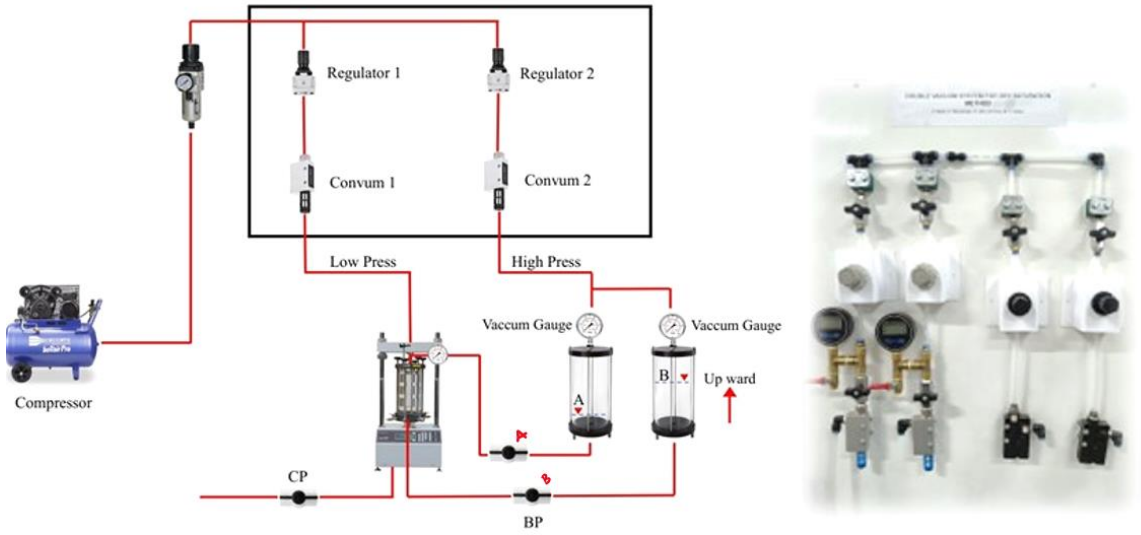

Figure 6. Schematic diagram of the double vacuum system method

Table 2. Scheme for applying vacuum pressure in the double vacuum method

Stage-n	Outside pressure (kPa)	Inside pressure (kPa)	Duration approx. (min.)
I	0	-20	±10
II	-20	-40	±10
III	-40	-60	±10
IV	-60	-80	±10
Elevate water tank B and maintain constant vacuum pressure for a total duration of ±4.5 hours or until water flows out of the drainage line of water tank A			
V	-40	-60	±10
VI	-20	-40	±10
VII	0	-20	±10

The influence of the double-vacuum system on the initial saturation process provided an initial pore pressure and a high B-value at the beginning of saturation, thereby accelerating the subsequent saturation process with the back-pressure system to achieve a B-value ≥ 95%.

Regarding the flushing duration, the results indicated that for short flushing times, the water flow entered the specimen/drainage system when the initial back pressure increased from 0 to +20 kPa. However, during prolonged flushing, the water flow was more likely to exit the specimen. Nevertheless, the initial flow direction does not always determine the degree of saturation, as in conventional saturation methods (such as the back-pressure method), in which water consistently flows out of the specimen. Regardless of the clay soil type, this outflow did not achieve complete saturation within a short time frame at low pressure. This phenomenon suggests that the specimens saturated using the back-pressure method had access to unlimited free water and may have undergone uncontrolled expansion.

Furthermore, this was confirmed through observations of deformation during the saturation and reconsolidation processes. The change in the height of the clean specimen during the back-pressure process was greater and more compressive than that in the double-vacuum method. Consequently, the volumetric change during saturation obtained using the back-pressure method was significantly larger than that obtained with the double-vacuum method. This indicated that the specimens saturated using the back-pressure method were predicted to have undergone a high degree of disturbance.

2.5. Triaxial Consolidated Undrained (TRXCU)

Triaxial consolidated undrained (TRXCU) testing was conducted in accordance with ASTM D4767-11 [18] using a triaxial stress path apparatus from GDS Instrument, Ltd. The United Kingdom integrated with a double-vacuum system, as shown in Figure 7. The load applied to the sample was recorded using a submersible load cell (5 kN capacity) situated within the triaxial chamber positioned above the top cap of the specimen. Consequently, the recorded data were not influenced by the frictional forces between the piston and chamber. This load cell exhibited an accuracy of 0.1% of its total capacity, which is equivalent to ±5N. Thus, for a sample with a diameter of 70 mm, the accuracy is within 1 kPa. The piston was maintained in a docked position to measure deformation from the onset of saturation. This configuration enables the piston to move in response to deformation during saturation, consolidation, and shear processes.

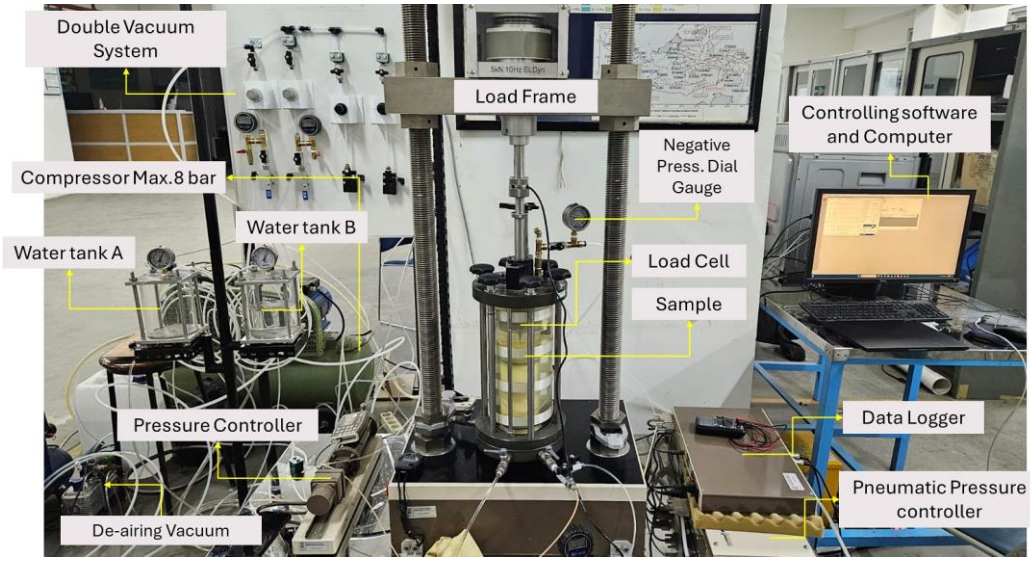

Figure 7. Schematic diagram of the triaxial apparatus integrated with a double vacuum system

Internal back pressure was applied using de-aired water, controlled by a GDS Digital Pressure Volume Controller. This controller is a microprocessor-controlled linear actuator designed to regulate and measure fluid pressure and volume changes precisely. The device was connected to a computer for automated control by using a general-purpose interface bus (GPIB). Pore water pressure was measured separately using a pore pressure transducer mounted on the specimen's base plate. The cell pressure was applied using the air pressure from a compressor regulated by a pneumatic controller.

Radial deformation was calculated based on the volume change recorded by the GDS digital pressure–volume controller. The magnitude of the radial deformation was analyzed from the radial strain value e_h, which is expressed as:

$$\varepsilon_h = \frac{\overline{\Delta D}}{D_o} \times 100\% \quad (1)$$

where: $\overline{AD}$ = Average diameter change; D_o= Initial diameter.

The average change in the diameter was calculated as follows:

$$\overline{\Delta D} = \left(\sqrt{\frac{A_n}{\pi}} \times 2\right) - D_0 \quad (2)$$

where: A_n = Current area; In the current area, A_n is given by:

$$A_n = \frac{(\pi x \times (D_o/2)^2 \times H_0) + \Delta V}{H_0 - \Delta H} \quad (3)$$

where: H_o = Initial height of sample; DV= volume change; DH = Height change.

2.5.1. Consolidation Stage

After determining B ≥ 0.95 at the final back pressure, isotropic consolidation was automatically performed on the specimen with a 70 mm diameter and a 140 mm height, using filter paper side drains around the perimeter. The specimens were isotropically consolidated under different pressures, and the isotropic consolidation process was continued for 24 h or until at least 98% of the excess pore water pressure dissipated. The consolidation stage was considered complete when the pore water drainage rate was less than 1 mm^3/min [25].

2.5.2. Undrained Shear

After automatic reconsolidation, undrained triaxial compression was conducted at an axial strain rate of 0.06 mm/min. The data were automatically recorded every 10 seconds. Once the test was completed, reaching a maximum axial strain of approximately 25%, the specimens were removed from the triaxial cell, and their water content was subsequently measured.

2.6. Micro-computed Tomography (micro-CT)

Micro-CT scanning of the four soil samples was performed using a Bruker Micro-CT SkyScan 1173 High Energy Micro-CT (see Figure 8), which was meticulously configured to capture high-resolution volumetric data. This device was suitable for scanning high-density samples. A total of 1800 projection images were acquired over 3 h, 30 min, and 10 s. The X-ray source was operated at 130 kV and 61 µA, with a 0.25 mm brass filter to optimize the beam quality. The camera was set to a 1 × 1 binning and captured images with a pixel size of 35 µm. To ensure data integrity, frame averaging (four frames) and random movement (10 steps) were performed. A complete 360-degree rotation was employed with a 0.200-degree rotation step in a step-and-shoot trajectory, ensuring comprehensive angular sampling.

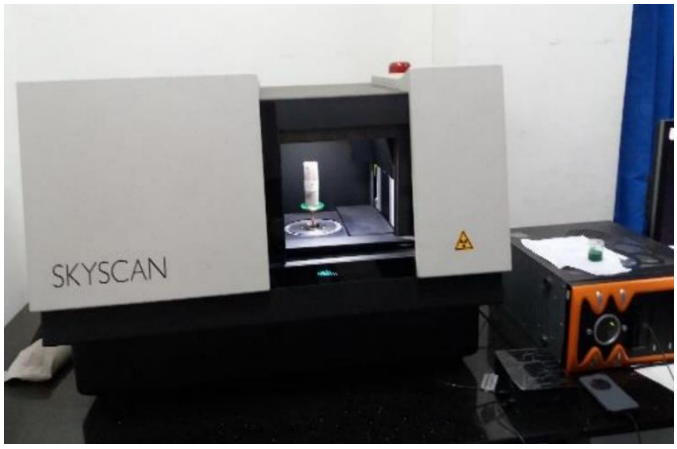

Figure 8. X-Ray micro-computed tomography (micro-CT) Bruker Skyscan 1173

Following the data acquisition, the raw projection images were reconstructed into 3D volumes using the NRecon program, version 1.7.4.6, powered by the GPU ReconServer engine (version 1.7.4) for accelerated processing. The reconstruction process, which took approximately 40 minutes for 1800 slices, produced output images with a resolution of 2160 × 2160 pixels and a pixel size matching that of the acquisition at 35 µm. A post-alignment correction of -0.50 was applied to refine the reconstruction accuracy.

To mitigate common CT artifacts, specific correction parameters were employed: a ring artifact correction level of 7 was applied, and the beam hardening correction was set at 25%. The conversion from CT numbers to image intensity was carefully calibrated to the minimum and maximum values of 0.001600 and 0.015000, respectively, to ensure accurate representation of material densities in the soil samples. The final reconstructed images were saved in BMP format, providing a robust dataset for subsequent analysis of the soil's internal structure.

3. Results and Discussion

3.1. Effect of the Double-vacuum Method on the Saturation Process

To investigate the influence of the double-vacuum method on the saturation process, saturation was performed on compacted kaolin samples using the back-pressure method (NV) and the double-vacuum method (DV). As shown in Figure 9, the results indicated that to achieve a Skempton B value ≥ 0.95, the NV method required a maximum pressure of 450 kPa. Figure 10 illustrates that the NV method requires approximately 50 h (more than 2 days, but no more than 3 days). In contrast, with the DV method, a Skempton B-value ≥ 0.95 could be achieved at a maximum pressure of 150-200 kPa within an average of 8 h. This aligns with the findings of Yin et al. [11, 28] , indicating that granite residual

soil requires 6 hours for vacuum saturation at a maximum back-pressure of 300 kPa (B-value ≥ 0.97). The variation in duration and maximum back-pressure is attributed to differences in sample diameter, Skempton B-Value target, volume void, and specimen microstructure. Meanwhile, the results differ between the NV and DV methods because of the vacuum process that removes soil pore air. Flushing with de-aired water from the bottom fills voids and forces air bubbles out of the top of the specimen. This process speeds up saturation in the DV method compared to the NV method.

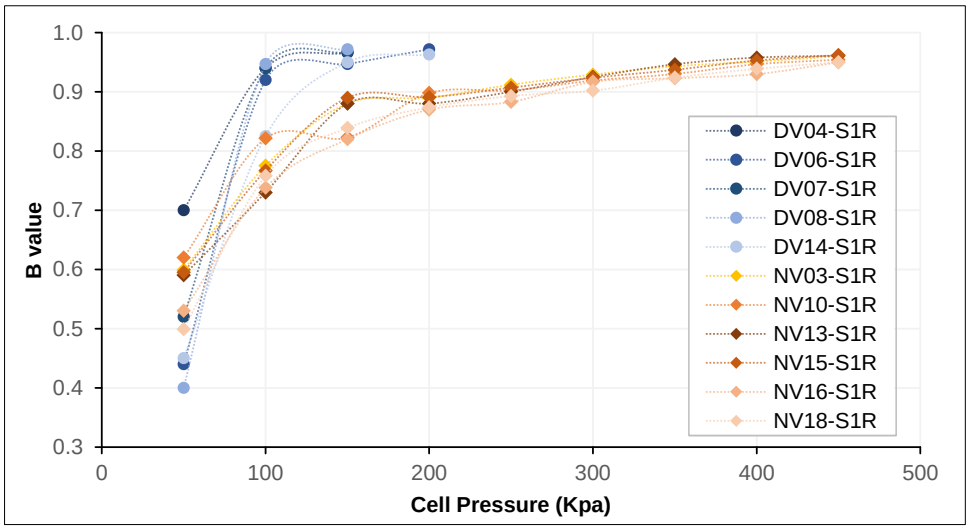

Figure 9. Skempton B-value and maximum saturation pressure in the NV and DV methods

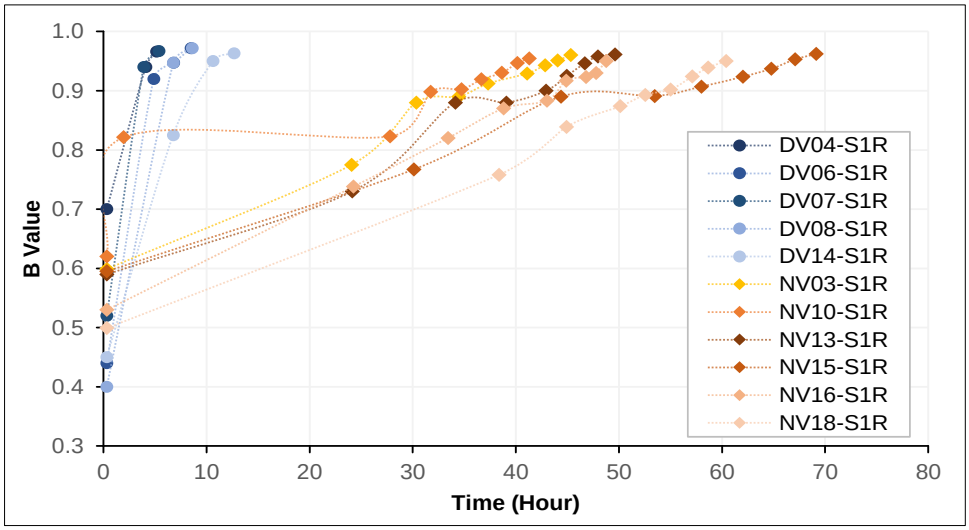

Figure 10. The time required to achieve B-value ≥ 0.95 for the NV and DV methods

To determine the real-time axial deformation during saturation and reconsolidation, the axial control function in the GDS triaxial program is set to a constant load cell value of zero. Under these conditions, the load frame maintained the internal load cell reading at zero. Thus, if the sample was enlarged, the internal load cell was compressed to 0 kN, prompting the load frame to automatically retract the piston until the internal load cell reading returned to 0 kN. By contrast, if the sample shrinks, the internal load cell is pulled and measures less than 0 kN, causing the load frame to automatically advance its piston until the internal load cell reading returns to 0 kN. This process occurs in real time with precision using the Proportional-Integrative- Derivative (PID) algorithm in the GDS triaxial program.

Figure 11 illustrates that the axial deformation of the kaolin clay samples resulting from the saturation process through the reconsolidation process, with an effective stress of 50 kPa using the DV method, generated a smaller net axial deformation (e_{vt} = ±0.9%) than the NV method (e_{vt} = ±1.8%). In other words, the axial deformation obtained using the NV method is nearly twice that obtained using the DV method. This discrepancy is attributed to the saturation process in the NV method, which requires a longer and repeated water-flushing time to achieve a B-value ≥ 0.95. Additionally, it necessitates repeated increases in back pressure and cell pressure to compress the air within the soil and facilitate its diffusion into water. Excessive water access using this method can lead to uncontrolled soil expansion. In contrast, the DV method uses a vacuum process to extract air from soil pores. Consequently, during flushing, the water

flowing from the bottom of the specimen fills the air voids. It pushed out the remaining air bubbles (caused by a vacuum pressure still significantly lower than atmospheric pressure) from the top of the specimen. Therefore, when applying the back pressure, repeated pressure increases were not needed to reach a B value of 0.95 or greater.

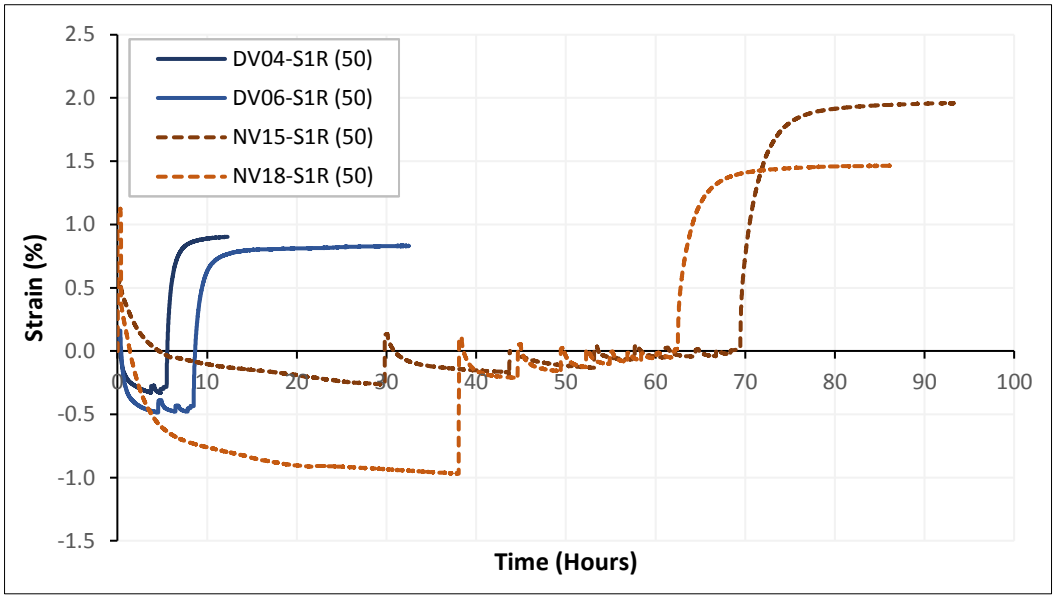

Figure 11. Axial deformation of kaolin clay due to saturation and reconsolidation process (σ'_v = 50 kPa) based on NV and DV methods

Applying a vacuum pressure close to atmospheric pressure (-90 kPa) will result in a faster saturation time and a lower final pressure than observed in this study. However, using high-capacity compressors (>12 bar) requires a significant financial investment and is not commonly used in Indonesian soil-mechanics laboratories.

Figure 12 shows that the radial deformation of kaolin clay samples caused by saturation during reconsolidation at an effective stress of 50 kPa using the DV method resulted in a smaller net radial deformation (e_{ht} = ±1 - 1.3%) than the NV method (e_{ht} = ±2.4%). In other words, the radial deformation measured with the NV method was approximately twice that measured with the DV method. Generally, radial deformation caused by the saturation process through reconsolidation is greater than the axial deformation. It should be noted that in this study, the specimens were compacted to a water content of 30%, resulting in relatively low compressibility and void ratio. Undisturbed or reconstituted samples with high void ratios, high water content, and high compressibility are expected to cause greater axial deformation.

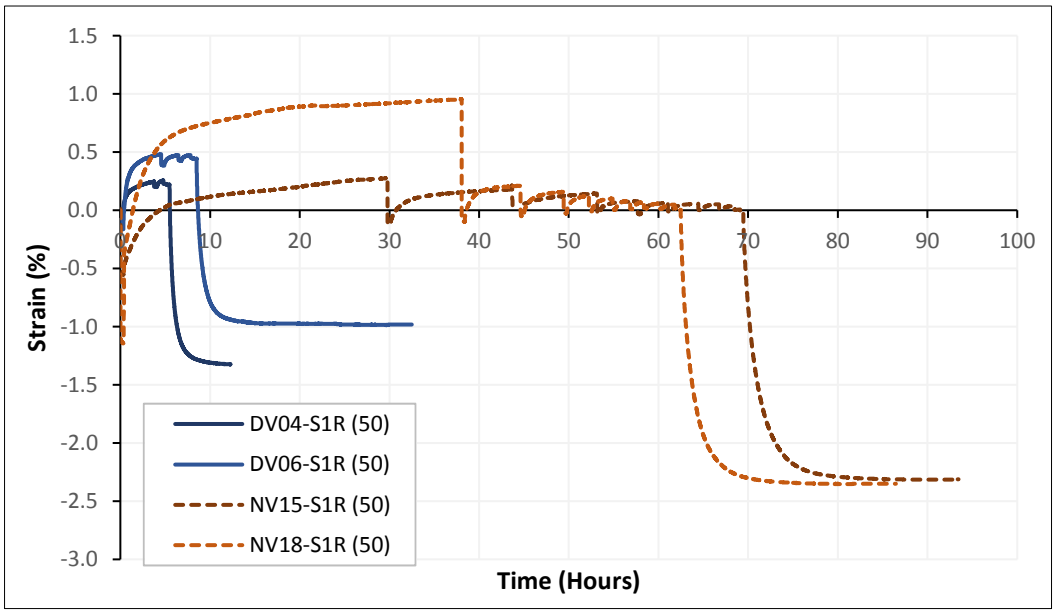

Figure 12. Radial deformation of kaolin clay due to saturation and reconsolidation process (σ'_v = 50 kPa) based on NV and DV methods

However, Liu et al. [45] stated that calculating radial deformation using the volume-change approach is inaccurate. Radial local measurements, such as LDT, LVDT, and Hall Effect, are recommended for better results. The limitations and availability of equipment were the main reasons for choosing the volume-change approach to calculate radial deformation in this study.

3.2. Effect of the Double-vacuum Method on Sample Disturbance

To determine the level of sample disturbance, Lunne et al. [9] proposed using the parameter $\Delta e/e_o$, where Δe represents the change in void ratio during the reconsolidation process towards the effective stress, and e_0 is the initial void ratio, as shown in Table 3. It should be noted that in their study, $\Delta e/e_o$ was measured using the oedometer test, which can lead to inaccurate De measurements when a gap exists between the specimen and the oedometer ring [46]. To account for these inaccuracies, the $\Delta e/e_o$ in this study was measured using a triaxial compression technique. The recompression technique can be applied if $\Delta e/e_o$ is less than 0.07. Therefore, it is impossible to overestimate the strength caused by poor sample quality in the recompression test, as long as the strength is not measured at very high strains. If only the residual effective stress is lost, the sample can be recovered using the recompression technique; however, if the soil structure is damaged, this technique cannot replicate the undisturbed soil behavior [15].

Table 3. Classification of sample quality based on void ratio changes during recompression [9]

Sample Quality and Process	Volume Change ($\Delta e/e_o$)
Very Good	< 0.04
Good to Fair	0.04 – 0.07
Fair to Poor	0.07 – 0.14
Very Poor	>0.14

As shown in Figure 13, the consolidation pressure test results at 50 kPa for all samples indicated that the NV Method produced a maximum $\Delta e/e_o$ value of ±0.09, which, according to Lunne et al. [9], indicates fair-to-poor sample quality. In contrast, the DV method produced a maximum $\Delta e/e_o$ value of ±0.055, which falls within the good-to-fair sample quality range. Teng & Ou [23] reported similar findings for reconstituted Taipei Silty clay soil, in which specimens saturated under suction are classified as "good to fair". In contrast, the quality of the specimens saturated without suction is classified as "fair to poor". This also indicates that, even without using localized measurement devices such as LDTs, LVDTs, or Hall-effect sensors, assessing changes in void ratio ($\Delta e/e_o$) during recompression still provides reasonably accurate results. It is predicted because the change in void ratio is determined by the variation in vertical strain, assuming the specimen maintains its cylindrical shape throughout the consolidation process (volumetric strain remains constant). Therefore, these findings suggest that specimens saturated with the NV method showed greater sample disturbance than those saturated with the DV method. During the saturation process, the NV method requires a specified number of incremental steps in cell pressure to achieve a B-value ≥ 0.95. This process results in the decomposition of particle bonds in soil, increasing the void volume. Consequently, during consolidation, the specimens saturated using the NV method exhibited greater compression than those saturated using the DV method.

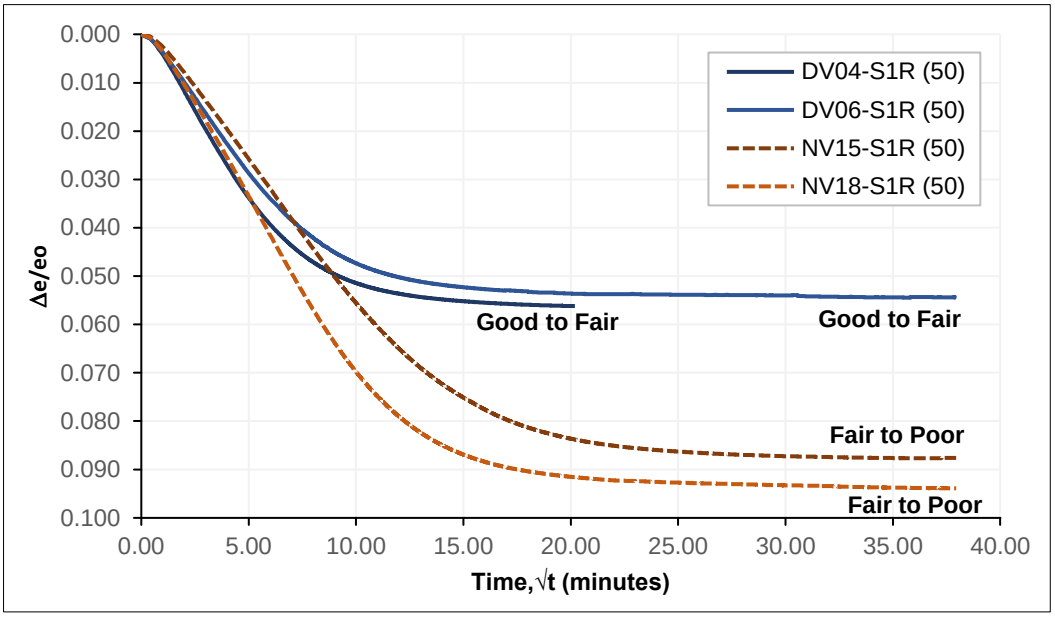

Figure 13. Effect of kaolin clay sample saturation process on sample disturbance (σ'_v = 50 kPa)

Furthermore, the suction pressure difference (-20 kPa) maintained during flushing in the double-vacuum method prevents significant expansion or compression of the specimen during increases in cell stress (Figures 10 and 11). The vacuum condition in the voids and the 70 cm hydraulic gradient in the DV method facilitated easier upward water flow through the specimen without requiring high diffusion pressures, as compared to the NV method. Based on these observations, it can be concluded that the saturation process has a greater impact on restoring the specimen to its original field condition than does the reconsolidation process. This result is consistent with observations made by Cho et al. [10].

3.2.1. Disturbance Based on Micro-computer Tomography (Micro-CT)

Following the scanning process, which generated a 16-bit TIFF image dataset, the reconstructed 8-bit grayscale BMP image datasets were analyzed. As shown in Figure 14, visualization using DataViewer (Bruker 3D Suite) reveals that both soil samples from the pre-saturation process exhibit striking visual structural similarities. They are characterized by aggregates of comparable size, homogeneously distributed throughout the entire volume of each sample. This suggested a consistent, granular, or clustered arrangement within the soil matrix, indicating a similar physical architecture between the two samples at the microscopic level, as resolved by the scan.

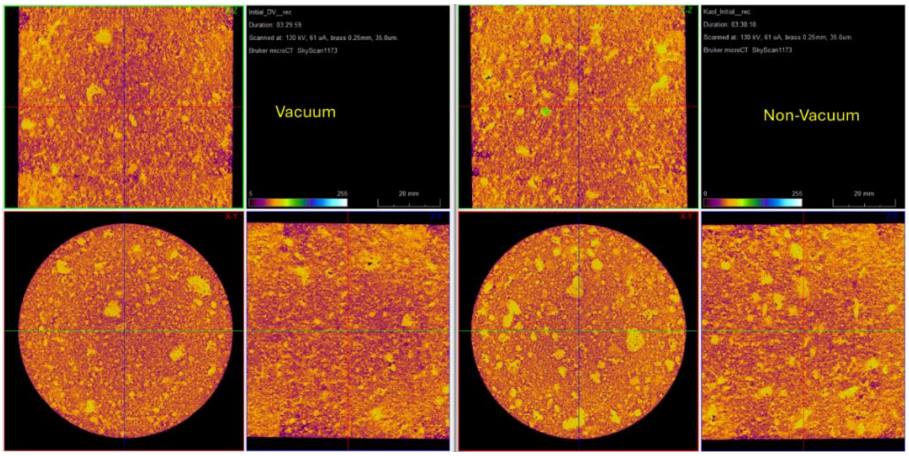

Figure 14. Qualitative analysis of the pre-saturation samples visualized using data viewer with pseudo-coloring features (Bruker 3D suite)

When subjected to pseudo-coloring based on the relative density, both samples predominantly displayed orange to yellow hues. This color range indicates that both samples fall within the low-to-medium density range. The dominance of these lighter colors suggests a less compact structure with potentially homogeneously distributed submicron pores or a lower concentration of high-density materials. This consistent density profile across the samples further reinforces their visual similarity in terms of overall material packing.

For scans of the post-saturation process, Figures 15 and 16 qualitatively show the difference in density. Following the saturation process, both soil samples exhibited an increase in density, as indicated by the shift to lighter, more yellow hues in the pseudo-colored scans. This color change suggests that the saturation treatment successfully introduced water into the pore spaces, thereby increasing the overall density of the materials within the samples.

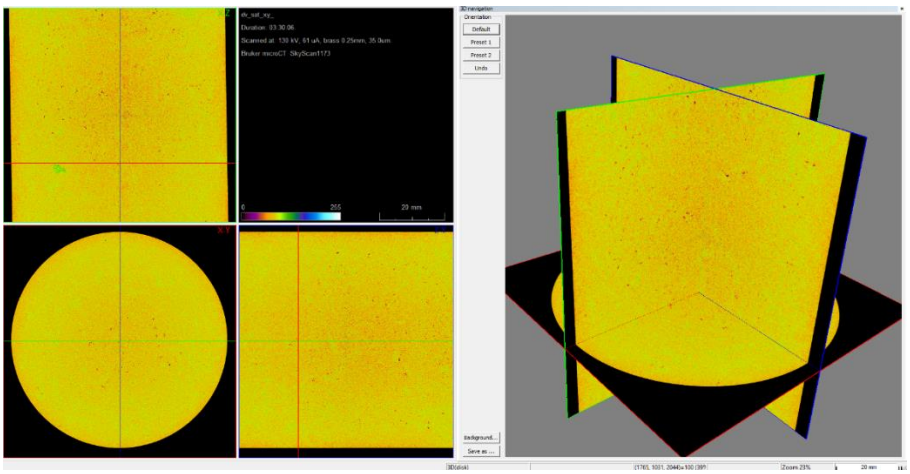

Figure 15. Qualitative analysis of the post-saturation samples vacuum sample as visualized using data viewer with pseudo-coloring features (Bruker 3D suite)

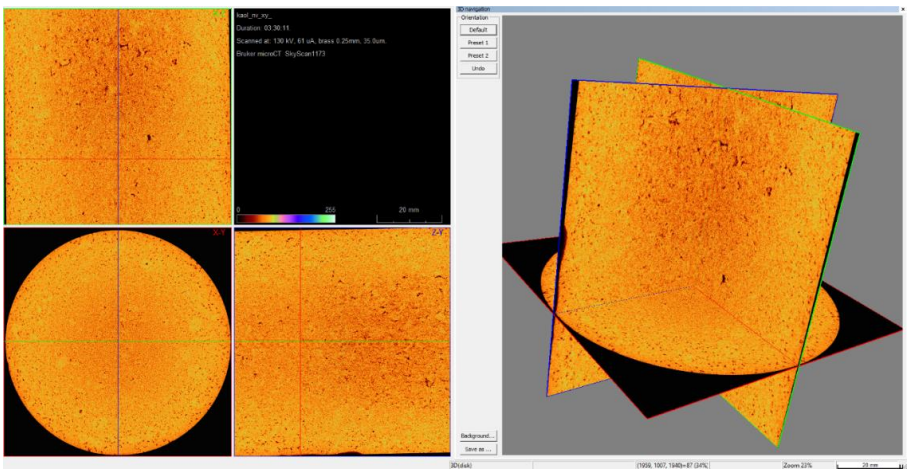

Figure 16. Qualitative analysis of the post-saturation non-vacuum samples as visualized using the data viewer with pseudo-coloring features (Bruker 3D suite)

The pseudo-coloring applied to the micro-CT images (Figures 14 to 16) depicts differences in sample density. The differences in pseudo-colour density maps are accurately presented because the sample sizes are the same and the acquisition and reconstruction parameters are kept constant across the samples, thereby maintaining consistency for further analysis and interpretation. The artifacts have been carefully compensated and reduced during preprocessing in the reconstruction process. Therefore, the color map can accurately depict density differences.

A notable difference in the structural homogeneity was observed between the two saturation methods. The non-vacuum-saturated (NV) sample exhibited a more heterogeneous structure than its double-vacuum-saturated (DV) counterpart. In the NV sample, pores were scattered with a tendency to concentrate towards the central and outer edges of the sample. In contrast, the DV sample showed a more even distribution of pores and fewer overall pores. This indicates that vacuum saturation achieved a more thorough and uniform filling of the pore network, resulting in a denser, more consistent internal structure, whereas non-vacuum saturation left pore spaces more unevenly filled.

Further quantitative analysis of the binarized micro-CT images provided a more precise understanding of the pore structures in both post-saturated samples. At a resolution of 35 µm per pixel, the detected pore volume fraction relative to the total cylindrical sample volume was significantly different: the NV sample exhibited a pore volume fraction of 1.04%, whereas the DV sample showed a considerably lower pore volume fraction of 0.43%. This directly confirms that the vacuum saturation process resulted in a substantially smaller detectable pore volume compared with the non-vacuum method, indicating a more effective filling of the pore network.

Previous qualitative analyses, as well as the calculation of 3D bulk porosity, are consistently supported by the 2D pore fraction analysis from Orthogonal Cross-Sections of the binarized images presented in Figures 17 and 18. Figure 17 illustrates the pore fraction observed across the horizontal cross sections (i.e., horizontal x-y slicing planes). The graph clearly demonstrates that across all vertical positions, the overall pore fraction of the vacuum-saturated sample remained consistently smaller than that of the non-vacuum-saturated sample. This consistent pattern along the vertical axis underlines the thoroughness and uniformity of the pore filling achieved by vacuum saturation, highlighting its superior ability to reduce residual air voids within the soil matrix compared with the non-vacuum approach.

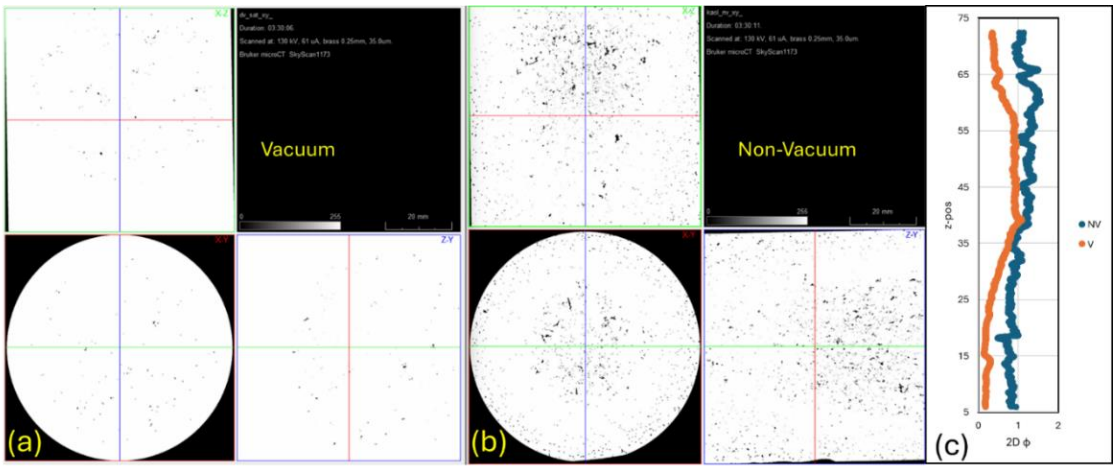

Figure 17. Binarized image of the Vacuum (a) and Non-Vacuum (b) samples utilized in a further analysis of the porosity. The 2D porosity plot of vertically sliced images (horizontal plane) for both samples

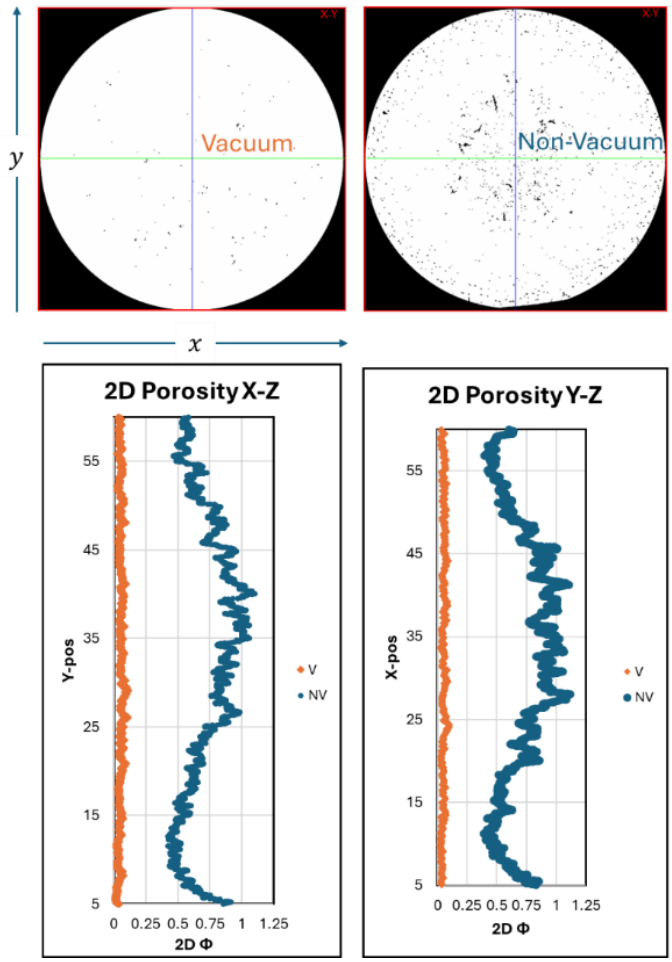

Figure 18. The 2D porosity analysis of the horizontally sliced images (vertical planes) from both samples, sliced in X-Z planes and Y-Z planes

As illustrated in Figure 18, the 2D pore fraction was further analyzed using graphs derived from two distinct slicing orientations. This provided a comprehensive view of pore distribution beyond the previously discussed horizontal (x-y) planes, i.e., the 2D XZ porosity was calculated from slices along the XZ plane, which are parallel to the green line (representing the front-to-back direction, or the y-axis); the 2D YZ Porosity was calculated from slices along the YZ plane, which are parallel to the blue line (representing the left-to-right direction or the x-axis).

From these analyses, it is evident that the pore space distribution is notably more homogeneous in the DV sample across both vertical slicing planes. This indicates that the vacuum saturation process not only reduced the total pore volume but also more evenly distributed the remaining pores throughout the sample, thereby avoiding the localized concentrations observed in the non-vacuum sample. Furthermore, these findings are consistent with the earlier analysis of the horizontal cross sections, confirming that the overall porosity of the DV remains smaller than that of the NV, irrespective of the slicing orientation. This reinforces the conclusion that vacuum saturation is a more effective method for minimizing and uniformly distributing residual porosity within soil samples

3.3. Effect of Water Tank Elevation

Based on double-vacuum testing conducted by Ampadu & Tatsuoka [17] on clay soil, the height difference between water tanks A and B during flushing was 70 cm. Lim et al. [24] applied hydraulic gradient pressures of 1-2 m during flushing, whereas Yilmaz et al. [5] utilized 4 m. Consequently, a study was conducted to investigate the effects of the hydraulic gradient height resulting from differences in water tank height on specimen deformation, disturbance, damage levels, and stress–strain characteristics. Water tank heights of 70 cm, 100 cm, and 150 cm were tested to assess their impact on the sample's disturbance levels. As shown in Figures 19 and 20, the results indicated that water tank height differences of 70 cm, 100 cm, and 150 cm produced axial deformations of 0.75%, 1.25%, and 2.25-3.9%, respectively, and a $\Delta e/e_0$ ratio of 0.055, 0.063, and 0.08, respectively. Figure 21 illustrates that the maximum deviatoric stresses were 35 kPa, 37 kPa, and 43 kPa, respectively. These findings suggest that higher hydraulic gradient pressures between water tanks A and B resulted in a more rapid flow of water into the specimen. This phenomenon increases the total axial deformation during saturation, thereby increasing the disturbance to the specimen, as evidenced by the increasing $\Delta e/e_0$ ratio. The $\Delta e/e_0$ ratio at the end of the reconsolidation process indicates greater specimen compression and greater dissipation of excess pore-water pressure during consolidation under equivalent effective pressure. This causes the deviatoric stress to increase as the hydraulic gradient height increases.

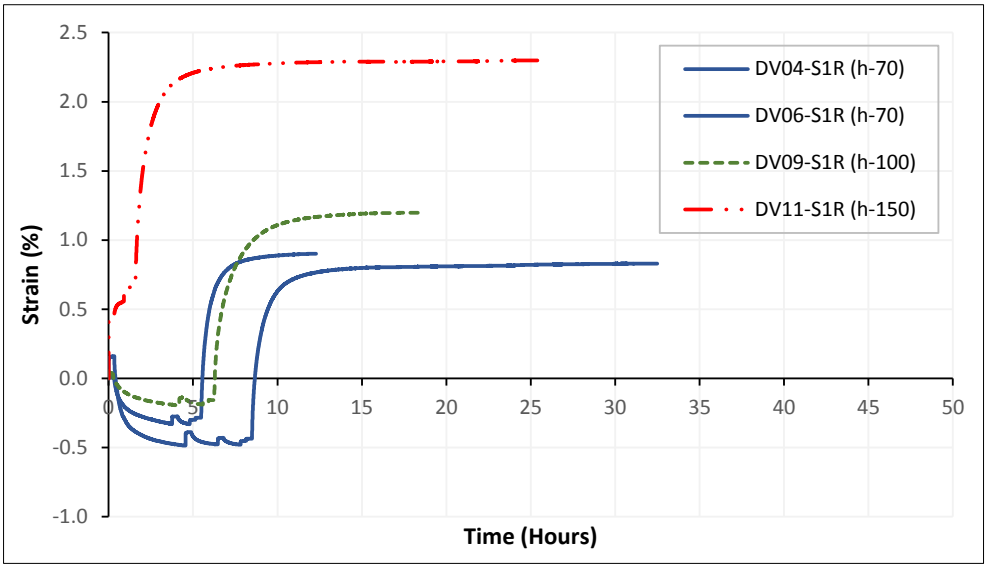

Figure 19. The influence of water tank elevation on axial deformation of kaolin clay in the DV method

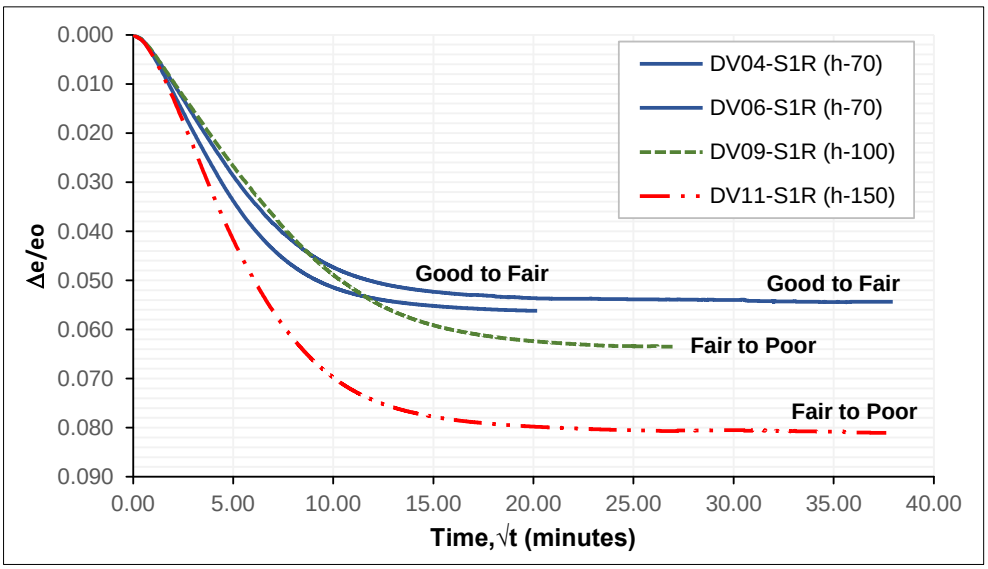

Figure 20. The influence of water tank elevation on the level of disturbance of the kaolin clay in the DV method

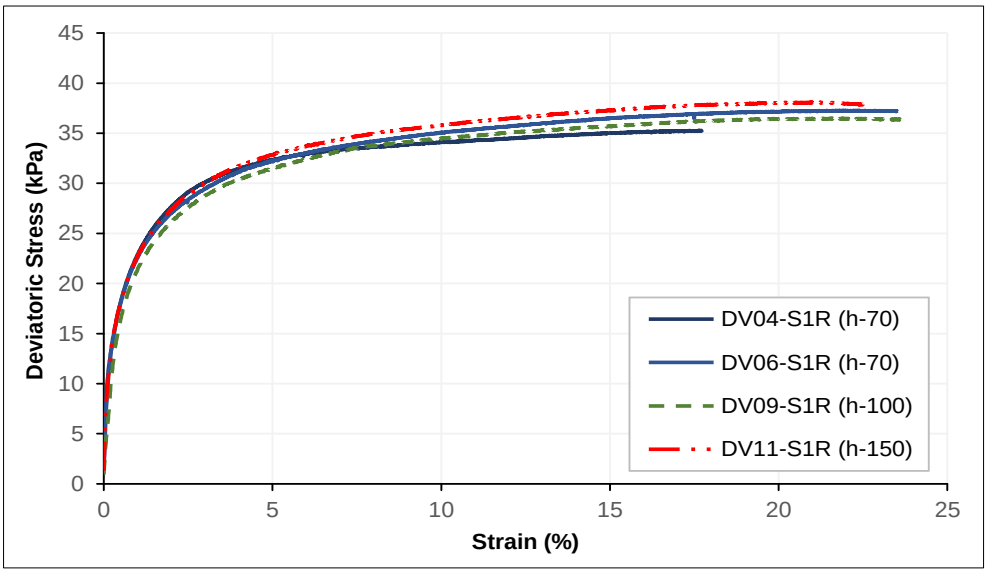

Figure 21. The influence of water tank height on the stress-strain curve of the kaolin clay in the DV method

3.4. Effect of Double-Vacuum Method on Stress-Strain Characteristics

The effect of saturation processes, using either the double-vacuum (DV) or back-pressure (NV) method, on the stress-strain characteristics was determined from triaxial consolidated undrained test results. As shown in Figure 22, the shearing results with a consolidation pressure of 50 kPa indicated that the saturation process using the back-pressure (NV) method generated a higher maximum deviatoric stress than the double vacuum (DV) method. This outcome is attributed to the repeated compression experienced by the sample in the back-pressure (NV) method, in contrast to that in the double vacuum (DV) method. Consequently, upon application of the reconsolidation pressure, the non-vacuum sample (NV) (using only the back-pressure method) underwent greater compression, resulting in a higher shear strength compared to the double vacuum saturation process, as shown in Figure 23.

Furthermore, Double Vacuum (DV) saturation results in a stress-path pattern that is more to the left relative to the non-vacuum (NV) method. This indicates a greater buildup of pore pressure, which reduces the effective stress more significantly than the non-vacuum (NV) method, as shown in Figure 24. This phenomenon occurs because the double-vacuum (DV) saturation process tends to maintain a more uniform pore-structure distribution than the non-vacuum (NV) method. As a result, drainage is more impeded, leading to a greater increase in pore pressure during shear than the non-vacuum (NV) method. The implication is that triaxial consolidated undrained test results obtained using the back-pressure method might overestimate results compared to those obtained with the double-vacuum method. However, because this study applied to compacted kaolin clay specimens with low initial void ratios, the differences in saturation methods did not significantly affect the effective shear strength values. Therefore, it is necessary to test undisturbed or reconstituted samples with high void ratios, water contents, and compressibility.

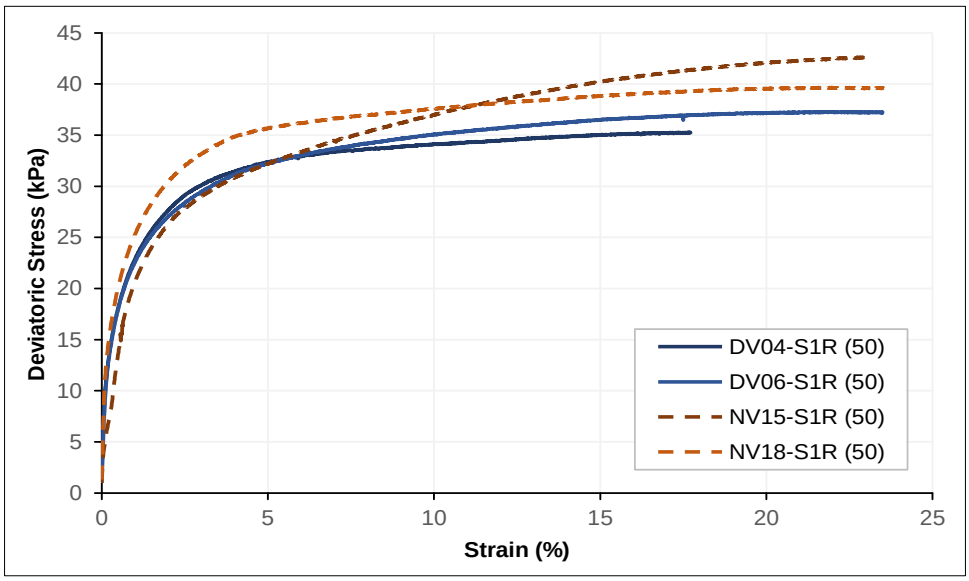

Figure 22. Influence of DV method vs. NV method on stress–strain relationship of kaolin clay sample

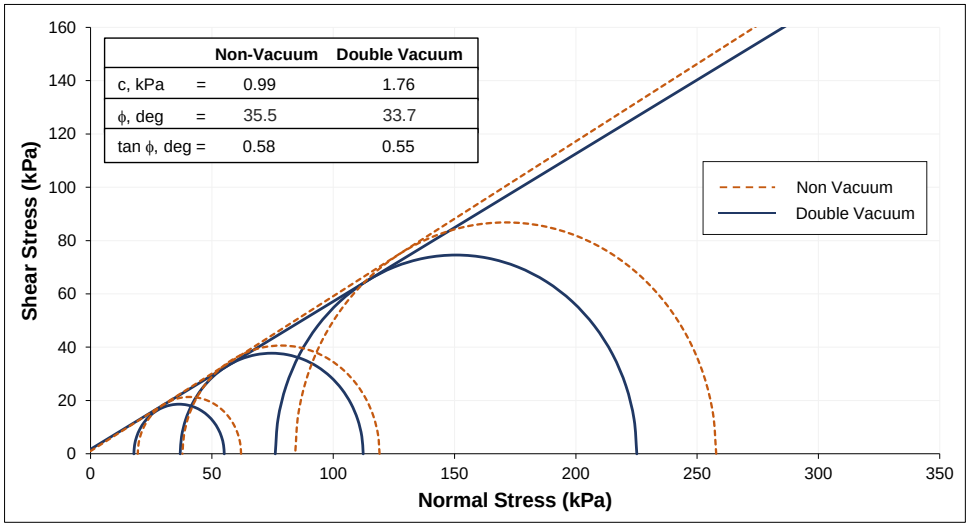

Figure 23. Influence of the DV method vs. the NV method on TRXCU test results for kaolin clay samples

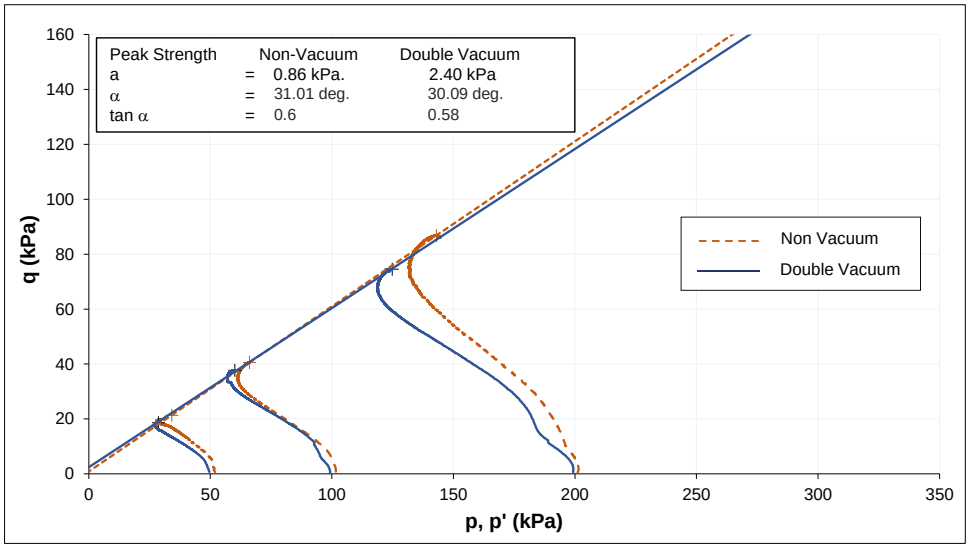

Figure 24. Stress path DV method vs. NV method for kaolin clay samples

4. Conclusions

Based on a study about sample disturbance on the application of the double vacuum saturation method in the triaxial consolidated undrained kaolin clay that has been carried out, it can be concluded as follows:

- The Double vacuum (DV) method reaches saturation of compacted Kaolin clay specimens faster, in about 9 hours, and at lower final pressure (150-200 kPa) compared to the back pressure (NV) method, which takes approximately 50 hours and requires higher pressure (450-700 kPa)
- The double-vacuum (DV) method results in significantly less axial and radial deformation in compacted kaolin clay specimens compared to the back-pressure (NV) method, with axial deformation nearly half as much and radial deformation also lower. However, the radial deformation measurement used in this study may be less accurate, and more reliable techniques such as LDT, LVDT, or Hall Effect sensors are recommended for future tests.
- The double vacuum (DV) saturation method causes less sample disturbance, ranging from good to moderate, compared to the back-pressure (NV) method, which results in moderate to poor disturbances. Overall, the DV method causes less sample damage during the saturation process.
- Based on micro-CT analysis, the overall porosity of the Double Vacuum (DV) method remained lower than that of the back-pressure (NV) method, regardless of the slicing orientation. This confirms that double vacuum (DV) saturation is a more effective way to reduce and evenly distribute residual porosity within soil samples.
- Applying a hydraulic gradient pressure exceeding 70 cm to compacted kaolin clay during the saturation process with the double-vacuum method caused significant axial deformation, increased sample disturbance, and higher deviatoric stress.
- Triaxial consolidated undrained testing showed that the Double Vacuum (DV) method produces lower deviatoric stress and shear strength compared to the back-pressure method, resulting in overestimated outcomes due to increased compression during reconsolidation. However, for compacted kaolin clay with low initial void ratios, the difference between the two methods did not significantly impact effective shear strength. Further testing of samples with higher void ratios and greater compressibility is recommended to understand this effect better.

4.1. Limitations

A limitation of this study is the use of compacted kaolin clay specimens with low initial void ratios and compressibility. Therefore, different saturation methods did not significantly impact the effective shear strength. Additionally, the high density and low void ratio lead to saturation-induced structural changes that are not easily visible. As a result, it is necessary to test undisturbed or reconstituted natural samples with higher void ratios, water contents, and compressibility. For soils sensitive to mineralogical changes, X-ray Diffraction (XRD) testing after saturation should be performed to identify mineralogical changes and subsequent cementation conditions. Local measurements of horizontal deformation were not conducted in this study. Future research should consider using local measurement techniques such as LDT or the Hall effect to observe changes in lateral deformation caused by the saturation process.

5. Declarations

5.1. Author Contributions

Conceptualization, M.R. and H.N.; methodology, M.R. and H.N.; validation, M.R., H.N., E.R., and F.D.E.L.; formal analysis, M.R.; investigation, M.R. and F.D.E.L.; data curation, M.R.; writing—original draft preparation, M.R. and F.D.E.L.; writing—review and editing, H.N.; supervision, H.N. and E.R. All authors have read and agreed to the published version of the manuscript.

5.2. Data Availability Statement

The data presented in this study are available on request from the corresponding author.

5.3. Funding

This research was supported and funded by the PPMI (Penelitian, Pengabdian, Masyarakat, dan Inovasi) period March-November 2024 from Institut Teknologi Bandung.

5.4. Acknowledgments

The Author wishes to acknowledge the GDS Advanced Triaxial Apparatus by the Soil Mechanics Laboratory, Department of Civil Engineering, Institut Teknologi Bandung. The Micro-CT laboratory at the Faculty of Mathematics and Natural Science, Institut Teknologi Bandung, is gratefully acknowledged.

5.5. Conflicts of Interest

The authors declare no conflict of interest.

6. References

[1] Donaghe, R. T., & Townsend, F. C. (1979). Effects of Back-Pressure Saturation Techniques on Results of R Triaxial Compression Tests. No. WESMPGL7912.

[2] Hossain, S. (2016). Effect of Drying-Wetting Cycles on Saturated Shear Strength of Undisturbed Residual Soils. American Journal of Civil Engineering, 4(4), 159. doi:10.11648/j.ajce.20160404.15.

[3] Lim, J. X., Chong, S. Y., Tanaka, Y., & Lee, M. L. (2018). Anisotropically Consolidated Undrained Compression Test on Residual Soil. E3S Web of Conferences, 65. doi:10.1051/e3sconf/20186506006.

[4] Wild, K. M., Barla, M., Turinetti, G., & Amann, F. (2017). A multi-stage triaxial testing procedure for low permeable geomaterials applied to Opalinus Clay. Journal of Rock Mechanics and Geotechnical Engineering, 9(3), 519–530. doi:10.1016/j.jrmge.2017.04.003.

[5] Yilmaz, Y., Kheirjouy, A. B., & Akgungor, A. P. (2016). Investigation of the effect of different saturation methods on the undrained shear strength of a clayey soil compacted with standard and modified proctor energies. Periodica Polytechnica Civil Engineering, 60(3), 323–329. doi:10.3311/PPci.8891.

[6] Fannin, R. J., & Slangen, P. (2014). On the distinct phenomena of suffusion and suffosion. Géotechnique Letters, 4(4), 289–294. doi:10.1680/jgele.15.00017.

[7] Hunter, R. P., & Bowman, E. T. (2018). Visualisation of seepage-induced suffusion and suffosion within internally erodible granular media. Geotechnique, 68(10), 918–930. doi:10.1680/jgeot.17.P.161.

[8] Zuo, L., Xu, L., Baudet, B. A., Gao, C., & Huang, C. (2020). The structure degradation of a silty loess induced by long-term water seepage. Engineering Geology, 272, 272. doi:10.1016/j.enggeo.2020.105634.

[9] Lunne, T., Berre, T., & Strandvik, S. (1997). Sample disturbance effects in soft low plastic Norwegian clay. In Symposium on Recent Developments in Soil and Pavement. Proceedings of the international symposium on recent developments in soil and pavement mechanics, 25-27 June, 1997, Rio de Janeiro, Brazil.

[10] Cho, W., Holman, T. P., Jung, Y.-H., & Finno, R. J. (2007). Effects of Swelling During Saturation in Triaxial Tests in Clays. Geotechnical Testing Journal, 30(5), 378–386. doi:10.1520/GTJ100797.

[11] Yin, S., Liu, P., Zhang, X., He, W., Yan, P., & Sun, Y. (2024). Field testing of shear strength of granite residual soils. Journal of Rock Mechanics and Geotechnical Engineering, 16(9), 3718–3732. doi:10.1016/j.jrmge.2023.11.034.

[12] Bjerrum, L. (1954). Geotechnical Properties of Norwegian Marine Clays. Géotechnique, 4(2), 49–69. doi:10.1680/geot.1954.4.2.49.

[13] Bjerrum, L., & Rosenqvist, I. TH. (1956). Some Experiments with Artificially Sedimented Clays. Géotechnique, 6(3), 124–136. doi:10.1680/geot.1956.6.3.124.

[14] Xu, X.-t., Shao, L.-j., Huang, J.-b., Xu, X., Liu, D.-q., Xian, Z.-x., & Jian, W.-b. (2021). Effect of wet-dry cycles on shear strength of residual soil. Soils and Foundations, 61(3), 782–797. doi:10.1016/j.sandf.2021.03.001.

[15] Tanaka, H. (2000). Sample quality of cohesive soils: Lessons from three sites, Ariake, Bothkennar and Drammen. Soils and Foundations, 40(4), 57–74. doi:10.3208/sandf.40.4_57.

[16] Rad, N. S., & Wayne Clough, G. (1984). New Procedure for Saturating Sand Specimens. Journal of Geotechnical Engineering, 110(9), 1205–1218. doi:10.1061/(asce)0733-9410(1984)110:9(1205).

[17] Ampadu, S. K., & Tatsuoka, F. (1993). Effect of setting method on the behaviour of clays in triaxial compression from saturation to undrained shear. Soils and Foundations, 33(2), 14–34. doi:10.3208/sandf1972.33.2_14.

[18] ASTM D4767-11. (2020). Standard Test Method for Consolidated Undrained Triaxial Compression Test for Cohesive Soils. ASTM International, Pennsylvania, United States. doi:10.1520/D4767-11.

[19] Nishimura, S., & Magalona, F. (2020). An alternative method in triaxial tests to obtain cross-anisotropic elastic parameters. Géotechnique Letters, 10(3), 468–477. doi:10.1680/jgele.20.00031.

[20] De Magistris, F. S., & Tatsuoka, F. (2004). Effects of moulding water content on the stress-strain behaviour of a compacted silty sand. Soils and Foundations, 44(2), 85–101. doi:10.3208/sandf.44.2_85.

[21] Wang, H., Koseki, J., Sato, T., Chiaro, G., & Tan Tian, J. (2016). Effect of saturation on liquefaction resistance of iron ore fines and two sandy soils. Soils and Foundations, 56(4), 732–744. doi:10.1016/j.sandf.2016.07.013.

[22] Lim, J. X., Tanaka, Y., Chong, S. Y., Ong, Y. H., & Lee, M. L. (2025). Mechanistic comparisons of MICP-treated residual soil and sand Part I: microstructural formation and deformation behaviour of soils. Discover Geoscience, 3(1), 85. doi:10.1007/s44288-025-00188-5.

[23] Teng, F. C., & Ou, C. Y. (2011). Application of a suction control system in the method of specimen saturation in triaxial tests. Geotechnical Testing Journal, 34(6), 34 102756. doi:10.1520/GTJ102756.

[24] Lim, J. X., Chong, S. Y., Tanaka, Y., & Lee, M. L. (2019). CI and CK0 Triaxial Tests for Tropical Residual Soil in Malaysia. First Malaysian Geotechnical Society (MGS) and Geotechnical Society of Singapore (GeoSS) Conference, 24-26 June, 2019, Petaling Jaya, Malaysia.

[25] Shu, R., Kong, L., Liu, B., & Wang, J. (2021). Stress–strain strength characteristics of undisturbed granite residual soil considering different patterns of variation of mean effective stress. Applied Sciences (Switzerland), 11(4), 1–16. doi:10.3390/app11041874.

[26] Li, L., Zang, M., Zhang, R., & Lu, H. (2023). Experimental Study on Mechanical Properties of Structured Clay under Different Unloading Rates and Unloading Stress Paths. Buildings, 13(6), 1544. doi:10.3390/buildings13061544.

[27] Li, L., Zang, M., Zhang, R. T., & Lu, H. J. (2022). Deformation and Strength Characteristics of Structured Clay under Different Stress Paths. Mathematical Problems in Engineering, 9266206. doi:10.1155/2022/9266206.

[28] Yin, S., Huang, J., Li, X., Sun, Y., Li, Y., & Zhang, X. (2025). Characteristics of wetting behavior under unloading in natural granite residual soil. Scientific Reports, 15(1), 7143. doi:10.1038/s41598-025-91749-8.

[29] Wang, Y., Jia, R., Li, Y., Yang, K., Cui, J., & Shan, Y. (2024). Study on the mechanical properties and microscopic evolution mechanisms of weathered granite soil. Scientific Reports, 14(1), 24388. doi:10.1038/s41598-024-75092-y.

[30] Lunne, T., Berre, T., Andersen, K. H., Strandvik, S., & Sjursen, M. (2007). Erratum: Effects of sample disturbance and consolidation procedures on measured shear strength of soft marine Norwegian clays. Canadian Geotechnical Journal, 44(1), 111. doi:10.1139/T07-008.

[31] Xu, P., Zhang, Q., Qian, H., Qu, W., & Li, M. (2021). Microstructure and permeability evolution of remolded loess with different dry densities under saturated seepage. Engineering Geology, 282, 282. doi:10.1016/j.enggeo.2020.105875.

[32] Zhang, L., Qi, S., Ma, L., Guo, S., Li, Z., Li, G., Yang, J., Zou, Y., Li, T., & Hou, X. (2020). Three-dimensional pore characterization of intact loess and compacted loess with micron scale computed tomography and mercury intrusion porosimetry. Scientific Reports, 10(1), 8511. doi:10.1038/s41598-020-65302-8.

[33] An, R., Kong, L., Zhang, X., & Li, C. (2022). Effects of dry-wet cycles on three-dimensional pore structure and permeability characteristics of granite residual soil using X-ray micro computed tomography. Journal of Rock Mechanics and Geotechnical Engineering, 14(3), 851–860. doi:10.1016/j.jrmge.2021.10.004.

[34] Zhuang, J., Kong, J., Zhu, Y., & Peng, J. (2024). The structural evolution of undisturbed loess due to water infiltration. Scientific Reports, 14(1), 14880. doi:10.1038/s41598-024-65838-z.

[35] Deng, J., Wang, L., Zhang, Z., & Bing, H. (2009). Microstructure characteristics and forming environment of late Quaternary Period loess in the Loess Plateau of China. Environmental Earth Sciences, 59(8), 1807–1817. doi:10.1007/s12665-009-0162-x.

[36] Shao, X., Zhang, H., & Tan, Y. (2018). Collapse behavior and microstructural alteration of remolded loess under graded wetting tests. Engineering Geology, 233, 11–22. doi:10.1016/j.enggeo.2017.11.025.

[37] Xie, X., Qi, S., Zhao, F., & Wang, D. (2018). Creep behavior and the microstructural evolution of loess-like soil from Xi'an area, China. Engineering Geology, 236, 43–59. doi:10.1016/j.enggeo.2017.11.003.

[38] Li, C., Kong, L., Shu, R., An, R., & Zhang, X. (2020). Disintegration characteristics in granite residual soil and their relationship with the collapsing gully in South China. Open Geosciences, 12(1), 1116–1126. doi:10.1515/geo-2020-0178.

[39] Li, H. Da, Tang, C. S., Cheng, Q., Li, S. J., Gong, X. P., & Shi, B. (2019). Tensile strength of clayey soil and the strain analysis based on image processing techniques. Engineering Geology, 253, 137–148. doi:10.1016/j.enggeo.2019.03.017.

[40] Hafez, M. A., Doris Asmani, M., & Nurbaya, S. (2010). Comparison between static and dynamic laboratory compaction methods. Electronic Journal of Geotechnical Engineering, 15, 1641–1650.

[41] Muntaha, M., Soemitro, R. A. A., & Warnana, D. D. (2016). The static and dynamic characteristic of undisturbed residual soils under drying-wetting cycle's repetition. Japanese Geotechnical Society Special Publication, 2(15), 591–594. doi:10.3208/jgssp.INA-04.

[42] Serratrice, J. F. (2022). Static compaction in laboratory of treated fine soils. 5th International Seminar on Earthworks in Europe, 21-22 April, 2022, Prague, Czech Republic.

[43] Albar, A., Osman, M. H., & Nyuin, J. D. (2022). Influence of membrane penetration on granitic residual soil in consolidated drained triaxial test. Physics and Chemistry of the Earth, Parts A/B/C, 128, 103254. doi:10.1016/j.pce.2022.103254.

[44] Junaideen, S. M., Tham, L. G., & Lee, C. F. (2021). Instability of Compacted Residual Soil. Geosciences, 11(10), 403. doi:10.3390/geosciences11100403.

[45] Liu, X.-Y., Wang, C.-M., Liu, H.-L., & Wu, D. (2022). An Experimental Investigation of the Mechanical Behavior and Particle Crushing Characteristic of Volcanic Soil. Materials, 15(15), 5423. doi:10.3390/ma15155423.

[46] Tanaka, H., & Tanaka, M. (2006). Main Factors Governing Residual Effective Stress for Cohesive Soils Sampled by Tube Sampling. Soils and Foundations, 46(2), 209–219. doi:10.3208/sandf.46.209.